〈Technical Note〉

DEVELOPMENT OF THE MULTI-DIMENSIONAL HYDRAULIC COMPONENT FOR THE BEST ESTIMATE SYSTEM ANALYSIS CODE MARS

SUNG WON BAE* and BUB DONG CHUNG
Korea Atomic Energy Research Institute
Mailbox 242, 150, Dukjin-dong, Yuseong-gu, Daejeon, 305-353, Korea
*Corresponding author. E-mail : bswon@kaeri.re.kr

Received April 15, 2009
Accepted for Publication September 4, 2009

A multi-dimensional component for the thermal-hydraulic system analysis code, MARS, was developed for a more realistic three-dimensional analysis of nuclear systems. A three-dimensional and two-fluid model for a two-phase flow in Cartesian and cylindrical coordinates was employed. The governing equations and physical constitutive relationships were extended from those of a one-dimensional version. The numerical solution method adopted a semi-implicit and finite-difference method based on a staggered-grid mesh and a donor-cell scheme. The relevant length scale was very coarse compared to commercial computational fluid dynamics tools. Thus a simple Prandtl's mixing length turbulence model was applied to interpret the turbulent induced momentum and energy diffusivity. Non drag interfacial forces were not considered as in the general nuclear system codes.

Several conceptual cases with analytic solutions were chosen and analyzed to assess the fundamental terms. RPI air-water and UPTF 7 tests were simulated and compared to the experimental data. The simulation results for the RPI air-water two-phase flow experiment showed good agreement with the measured void fraction. The simulation results for the UPTF downcomer test 7 were compared to the experiment data and the results from other multi-dimensional system codes for the ECC delivery flow.

KEYWORDS : Multi-dimension, MARS, System Code, Best Estimate

1. INTRODUCTION

In the early 1990's, the OECD 2D/3D program clearly demonstrated the need for a multi-dimensional analysis of nuclear reactor thermal-hydraulics [1]. The OECD has also placed importance on the multi-dimensional analysis capability as a requirement of the next generation safety codes [2]. Best-estimate system codes, such as TRACE, RELAP5-3D and CATHARE2 have been developed with multi-dimensional capabilities, and extensive experimental programs have been carried out [3-6]. These activities have improved the understanding of the two-phase flow phenomena that occur in current light water reactors under certain accident conditions.

In particular, many multi-dimensional issues have been raised regarding Korean PWR configurations and designs. The representative multi-dimensional phenomena surrounding the Korean PWR systems are summarized as:

- Upper plenum injection of low head ECCS (Emergency Core Cooling System)
- DVI (Direct Vessel Injection) water sweep out through the cold leg
- DVI penetration hesitation by downcomer vessel boiling
- IRWST (In-containment Refueling Water Storage Tank) water temperature increase.

These issues depend on the specific design configurations for the power plants. The UPI (Upper Plenum Injection) problem is concerned with the down flow and sweep out amounts of water from the coolant pool that forms on the top of the upper tie plate during LBLOCAs in UPI-type plants [7]. The water sweep-out problem also arises in the DVI configuration when cold leg break accidents are simulated. When the emergency coolant is injected through the DVI nozzle, chaotic water entrainment and spreading occurs inside the downcomer gap. If the cold leg is thought to be broken, the sweep-out amounts of the entrained and spread water through the broken cold leg are of great concern [8].

The downcomer vessel boiling phenomenon induces a hesitation of the emergency coolant downflow due to the upward bubble flows. The bubbles are generated on

the inside of the vessel wall. In a recent experiment, a circulation flow was created by an upward bubble and a downward water flow [9]. It is difficult to conduct a proper analysis of the circulation flow and obtain a feasible bubble rising velocity with traditional 1-D modeling. As a consequence, an overestimated void fraction and lack of water down flow in the downcomer region together lead to unwanted core fuel clad temperature behavior.

IRWST is a large water reservoir that is used to cool high-temperature steam in accident situations. The cool down capability and the temperature of the water pool are the key parameters for a prediction of the integrity of the containment [10]. It is not sufficient to model IRWST as a 1-D component due to of the induced water flow inside IRWST. This flow affects the cooling capacity and the water temperature behavior. For these phenomena, the lateral movement interpretations in relation to the coolant water and air or steam are the key parameters of successful accident predictions and analyses.

KAERI (the Korea Atomic Energy Research Institute) has developed the MARS code for multi-dimensional multi-purpose reactor safety [11,12]. In the MARS code, the RELAP5/MOD3 and COBRA-TF codes were merged as one-dimensional and three-dimensional vessel thermal-hydraulics modules, respectively. The MARS vessel module which is based on COBRA-TF uses a two-fluid, three-field model for two-phase flows in rectangular Cartesian or sub-channel coordinates. However, it is difficult to apply the MARS vessel module, to a general 3D flow field such as a cylindrical pool. In order to overcome these restrictions, a new multi-dimensional component was developed to allow more flexible multi-dimensional geometry descriptions. The multi-dimensional component uses a porous body approach. The multi-dimensional component is capable of carrying out multi-dimensional simulations in an open medium such as IRWST. In an open media simulation, MARS was implemented a simple Prandtl's mixing length-based viscosity term, of which the magnitude was determined by user input. This paper presents the development and a fundamental assessment of the multi-dimensional component of the MARS comparison with different experimental tests (RPI, UPTF).

2. BASIC EQUATIONS

The governing equations in the MARS multi-dimensional component are extended from the general two fluids porous body equations. There are many references for the derivation of multi-dimensional governing equations [5,13,14]. Among these, the RELAP5-3D code manual contains the porous body formulation [5]. RELAP5-3D, however, does not consider momentum exchanges by means of the viscous stress between control volumes in open media situations.

The governing equations of the MARS multi-dimensional component mainly follow RELAP5-3D. The virtual mass term is maintained in the multi-dimensional momentum equation. The wall friction term is activated if the concerned volume is in the neighborhood of the wall-confined boundary. However, for the internal volume of open media, the wall friction does not work. Instead, the viscous stress terms, which include the turbulent viscosity, are activated. A turbulent heat diffusion term is also added to the MARS multi-dimensional internal energy equation for the heat exchange between the internal volumes.

The control volume considered in this model is shown in Figure 1. V is the volume occupied by all phases and $V_f(t)$ is the volume occupied by fluid in the region of interest. $V_f(t)$ is surrounded surfaces $S_i(t)$ and S_c. Surface $S_i(t)$ is the interface between the phase in $V_f(t)$ and the other phase. Surface S_c is the fixed surface of interest. Surface $S_i(t)$ moves with velocity $\bar{v}_s$, whereas S_c is fixed, i.e., $\bar{v}_s = 0$ on S_c. Note that $\bar{v}_s$ is the velocity of the interface, not the fluid velocity, and $V_f(t)$ is a function of time because $S_i(t)$ is

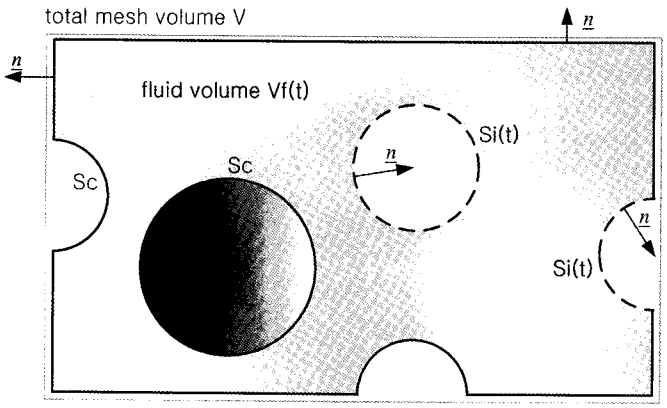

Sc: boundary of wall or neighboring meshes in piled volumes
Si(t): phase interface

Fig. 1. Control Volume for the Multi-dimensional Two-phase, Two-fluid Governing Equation

moving. Henceforth, *As* refers to the area of phase interface and *Aw* represents the area of the solid boundary wall.

The spatial integral form of the generalized phase balance equation is as follows:

$$\int_{V_k}\frac{\partial\rho_k\varphi_k}{\partial t}dV+\int_{V_k}\nabla\cdot\left(\rho_k\varphi_k\underline{v}_k\right)dV+\int_{V_k}\nabla\cdot\underline{\underline{J}}_k\,dV-\int_{V_k}\rho_k\phi_k dV=0 \quad (1)$$

The parameters of equation (1) are listed in Table 1.

After using the Leibnitz rule on the first term of the equation (1), and applying the Gauss theorem to the spatial divergence term of equation (1), the time derivative term and divergence terms are as follows:

$$\int_{V_k}\frac{\partial\rho_k\varphi_k}{\partial t}dV=\frac{\partial}{\partial t}\int_{V_k}\rho_k\varphi_k dV-\int_{A_s}\rho_k\varphi_k\underline{v}_s\cdot\underline{n}\,dA \quad \text{(Leibnitz Rule)} \quad (2)$$

$$\int_{V_k}\nabla\cdot\left(\rho_k\varphi_k\underline{v}_k+\underline{\underline{J}}_k\right)dV$$
$$=\nabla\cdot\int_{V_k}\left(\rho_k\varphi_k\underline{v}_k+\underline{\underline{J}}_k\right)dV+\int_{A_s}\left(\rho_k\varphi_k\underline{v}_k+\underline{\underline{J}}_k\right)\cdot\underline{n}\,dA+\int_{A_w}\left(\underline{\underline{J}}_k\right)\cdot\underline{n}\,dA$$
(Divergence Theorem) (3)

Where $\underline{v}_k\cdot\underline{n}=0$. Here, the area integration operates, i.e., as *As* or *Aw*.

Finally, inserting equation (2) and (3) into equation (1) gives

$$\frac{\partial}{\partial t}\left[\left(\frac{V_k}{V}\right)\frac{1}{V_k}\int_{V_k}\rho_k\varphi_k dV\right]+\left(\frac{1}{V}\right)\nabla\cdot\left[V\left(\frac{V_k}{V}\right)\left(\frac{1}{V_k}\right)\int_{V_k}\left(\rho_k\varphi_k\underline{v}_k+\underline{\underline{J}}_k\right)dV\right]$$
$$-\left(\frac{V_k}{V}\right)\left(\frac{1}{V_k}\right)\int_{V_k}(\rho_k\phi_k)dV+\left(\frac{1}{V}\right)\int_{A_s}\left[\rho_k\varphi_k\left(\underline{v}_k-\underline{v}_s\right)\cdot\underline{n}+\underline{\underline{J}}_k\cdot\underline{n}\right]dA$$
$$+\left(\frac{1}{V}\right)\int_{A_w}\underline{\underline{J}}_k\cdot\underline{n}\,dA=0 \quad (4)$$

Equation (4) is the control volume form of the phase balance equations for the general quantities.

The following definitions are derived considering the control volume shown in Figure 1:

Table 1. The Parameters of the Phasic Balance Equations

	φ_k	$\underline{\underline{J}}_k$	ϕ_k
Mass	1	0	0
Momentum	$\underline{v}_k$	$P_k\underline{\underline{I}}-\underline{\underline{\tau}}_k$	$\underline{g}$
Energy	$U_k+\underline{v}_k\cdot\underline{v}_k/2$	$q_k+(P_k\underline{\underline{I}}-\underline{\underline{\tau}}_k)\underline{v}_k$	$\underline{g}\cdot\underline{v}_k+Q_k/\rho_k$

- Area of the A_i flowing fluid phase under consideration : A_{ci}
- The volume average notation of phase k:$\langle f_k\rangle\equiv(1/V_k)\int_{V_k}f_k dV$
- The area and volume fraction of the fluid : $\gamma_a=A_{ci}/A$ and $\gamma_v=V_f(t)/V$
- The phase k fraction of V : $\alpha_k=V_k(t)/V_f(t)$
- The interface mass flux with phases : $\dot{m}_k\equiv\rho_k(\underline{v}_k-\underline{v}_s)\cdot\underline{n}$
- Flux term $\underline{\underline{J}}_k$ is expanded with the spatial and time average : $\underline{\underline{J}}_k=\langle\underline{\underline{J}}_k\rangle+\Delta\underline{\underline{J}}_k$

Using the definitions above, equation (4) becomes

$$\frac{\partial}{\partial t}\left[\gamma_v\langle\alpha_k\rho_k\varphi_k\rangle\right]+\left(\frac{1}{V}\right)\nabla\cdot\left[V\gamma_v\alpha_k\left\langle\rho_k\varphi_k\underline{v}_k+\underline{\underline{J}}_k\right\rangle\right]-\gamma_v\langle\alpha_k\rho_k\phi_k\rangle$$
$$=-\left(\frac{1}{V}\right)\int_{A_s}\left(\dot{m}_k\varphi_k+\underline{\underline{J}}_k\cdot\underline{n}\right)dA-\left(\frac{1}{V}\right)\int_{A_w}\underline{\underline{J}}_k\cdot\underline{n}\,dA \quad (5)$$

The terms related to $\underline{\underline{J}}_k$ on the right side of equation (5) are divided to the spatial and time average terms. The following equations are derived by applying the Gauss theorem:

$$\int_{A_s}\underline{\underline{J}}_k\cdot\underline{n}\,dA+\int_{A_w}\underline{\underline{J}}_k\cdot\underline{n}\,dA$$
$$=\left\langle\underline{\underline{J}}_k\right\rangle\cdot\left[\int_{A_s}\underline{n}\,dA+\int_{A_w}\underline{n}\,dA\right]+\int_{A_s}\Delta\underline{\underline{J}}_k\cdot\underline{n}\,dA+\int_{A_w}\Delta\underline{\underline{J}}_k\cdot\underline{n}\,dA$$
$$=\int_{A_s}\Delta\underline{\underline{J}}_k\cdot\underline{n}\,dA+\int_{A_w}\Delta\underline{\underline{J}}_k\cdot\underline{n}\,dA \quad (6)$$

Thus, equation (5) is obtained like in the following form:

$$\frac{\partial}{\partial t}\left[\gamma_v\langle\alpha_k\rho_k\varphi_k\rangle\right]+\left(\frac{1}{V}\right)\nabla\cdot\left[V\gamma_v\alpha_k\left\langle\rho_k\varphi_k\underline{v}_k+\underline{\underline{J}}_k\right\rangle\right]-\gamma_v\langle\alpha_k\rho_k\phi_k\rangle$$
$$=-\left(\frac{1}{V}\right)\int_{A_s}(\dot{m}_k\varphi_k)dA-\left(\frac{1}{V}\right)\int_{A_s}\Delta\underline{\underline{J}}_k\cdot\underline{n}\,dA-\left(\frac{1}{V}\right)\int_{A_w}\Delta\underline{\underline{J}}_k\cdot\underline{n}\,dA \quad (7)$$

Here, γ_v is the volume porosity. Equation (7) is the resultant control volume form of the general phase balance equation. The multi-dimensional momentum and energy equations are obtained through the equation (7).

Inserting the momentum equation parameters in Table 1 into equation (7), the equation (8) is created.

$$\gamma_v\frac{\partial}{\partial t}\langle\alpha_k\rangle\langle\rho_k\rangle\langle\underline{v}_k\rangle+\left(\frac{1}{V}\right)\nabla\cdot\left[V\gamma_v\langle\alpha_k\rangle\langle\rho_k\rangle\langle\underline{v}_k\underline{v}_k\rangle\right]$$
$$+\left(\frac{1}{V}\right)\nabla\cdot\left[V\gamma_v\langle\alpha_k\rangle\left(\langle P_k\underline{\underline{I}}\rangle-\langle\underline{\underline{\tau}}_k\rangle\right)\right]-\gamma_v\langle\alpha_k\rangle\langle\rho_k\rangle\underline{g}$$
$$=\Gamma_k\underline{v}_k-\left(\frac{1}{V}\right)\int_{A_s}\left(\Delta P_k\underline{\underline{I}}-\Delta\underline{\underline{\tau}}_k\right)\cdot\underline{n}\,dA-\left(\frac{1}{V}\right)\int_{A_w}\left(\Delta P_k\underline{\underline{I}}-\Delta\underline{\underline{\tau}}_k\right)\cdot\underline{n}\,dA \quad (8)$$

In this equation, Γ_k is the interfacial k phase mass flux per unit volume.

The next step involves dropping the spatial average notation < > for the density and volume fraction of the k phase based on the constant profile assumption in the concerned volume. The interfacial momentum storage $\Gamma_k \underline{v}_k$ is neglected. The integration terms on the right side are at this point performed on the interface area and the wall area. The shear stress terms acting on the interface and the wall become the frictional forces per unit volume, which have the same meaning for MARS and REALP5 [16]. Assuming that the phase pressure is equal to the interfacial pressure, equation (8) is as follows:

$$\gamma_v \frac{\partial}{\partial t}\alpha_k\rho_k\underline{v}_k + \left(\frac{1}{V}\right)\nabla\cdot\int_{V_k}\alpha_k\rho_k\underline{v}_k\underline{v}_k dV + \gamma_v\nabla\cdot\alpha_k P$$
$$= \gamma_v\alpha_k\rho_k\underline{g} + \left(\frac{1}{V}\right)\nabla\cdot\int_{V_k}\alpha_k\left(\underline{\underline{\tau}}+\underline{\underline{\tau}}^T\right)dV - \gamma_v F_i - \gamma_v F_w \quad (9)$$

The convection and diffusion terms in equation (9) are rearranged as follows based on the constant assumption of the density and volume fraction of phase k,

$$\left(\frac{1}{V}\right)\nabla\cdot\int_{V_k}\alpha_k\rho_k\underline{v}_k\underline{v}_k dV = \frac{1}{V}\int_{A_k}\alpha_k\rho_k\underline{v}_k(\underline{v}_k\cdot\underline{n})dA$$
$$= \frac{A}{V}\left\{\left[\gamma_a\alpha_k\rho_k\underline{v}_k(\underline{v}_k\cdot\underline{n})\right]_{A_k+} - \left[\gamma_a\alpha_k\rho_k\underline{v}_k(\underline{v}_k\cdot\underline{n})\right]_{A_k-}\right\}$$
$$= \nabla\left(\gamma_a\alpha_k\rho_k\underline{v}_k\underline{v}_k\right) \quad (10)$$

$$\left(\frac{1}{V}\right)\nabla\cdot\int_{V_k}\alpha_k\left(\underline{\underline{\tau}}+\underline{\underline{\tau}}^T\right)dV = \frac{1}{V}\int_{A_k}\alpha_k\underline{\underline{\tau}}'\cdot\underline{n}\,dA$$
$$= \nabla\left[\gamma_a\alpha_k\underline{\underline{\tau}}'\right] \quad (11)$$

where the shear stress $\underline{\underline{\tau}}'(=\underline{\underline{\tau}}+\underline{\underline{\tau}}^T)$ includes the turbulent shear as well as the normal viscous shear. Equation (12) is finally obtained as the momentum equation of phase k.

$$\gamma_v\frac{\partial}{\partial t}\alpha_k\rho_k\underline{v}_k + \nabla\left(\gamma_a\alpha_k\rho_k\underline{v}_k\underline{v}_k\right) + \gamma_v\nabla\cdot\alpha_k P$$
$$= \gamma_v\alpha_k\rho_k\underline{g} + \nabla\left(\gamma_a\alpha_k\underline{\underline{\tau}}'\right) - \gamma_v F_i - \gamma_v F_w \quad (12)$$

Dividing the volume porosity and ignoring the non-drag interfacial forces, the final x-directional momentum equation for the gas phase can be induced as equation (13). In this equation, the frictional terms and virtual mass terms use the same notational form as the one-dimensional equations of RELAP5 or MARS. The source and function of the virtual mass term were well described well an earlier study [5].

$$\alpha_g\rho_g\frac{\partial u_g}{\partial t} + \frac{1}{\gamma_v}\left(\frac{1}{2}\alpha_g\rho_g\gamma_{a,x}\frac{\partial u_g^2}{\partial x} + \alpha_g\rho_g\gamma_{a,y}v_g\frac{\partial u_g}{\partial y} + \alpha_g\rho_g\gamma_{a,z}w_g\frac{\partial u_g}{\partial z}\right)$$
$$= -\alpha_g\frac{\partial P}{\partial x} + \alpha_g\rho_g B_x - \alpha_g\rho_g(FWG)u_g + \Gamma_g(u_{gI}-u_g) - \alpha_g\rho_g(FIG)(u_g-u_f)$$
$$-C\alpha_g\alpha_f\rho_m\left[\frac{\partial(u_g-u_f)}{\partial t} + u_f\frac{\partial u_g}{\partial x} - u_g\frac{\partial u_f}{\partial x}\right]$$
$$+\frac{\alpha_g(\mu_g+\mu_{g,T})}{\gamma_v}\left[\gamma_{a,y}\frac{\partial^2 u_g}{\partial y^2} + \gamma_{a,z}\frac{\partial^2 u_g}{\partial z^2}\right] \quad (13)$$

The last turbulent mixing term comes from the τ' component in equation (11). The $\partial/\partial x$, $\partial/\partial y$, and $\partial/\partial z$_terms refer to the directional derivatives. In the multi-dimensional momentum equation, the non-drag interfacial forces of the bubble lift force, the wall-lubrication force, and the bubble dispersion force are ignored.

As with the phase balance equations (7), the energy equations are derived from the parameters in Table 1. After inserting the energy equation parameters into equation (7), excepting the mechanical energy term and ignoring the averaging notation, the balance equation become

$$\partial(\rho_k U_k)/\partial t + \nabla\cdot(\rho_k U_k\underline{v}_k) = -\nabla\cdot\underline{q}_k - \left(P_k\underline{\underline{I}} - \underline{\underline{\tau}}_k\right):\nabla\underline{v}_k + Q_k \quad (14)$$

where $\underline{q}_k$ is the heat addition through the interface and bounding wall. Q_k_ is the direct volumetric heating. By Intergrating the above equation for the volume of phase k, it can be rewritten in the following form.

$$\int_{V_k}\frac{\partial\rho_k U_k}{\partial t}dV + \int_{V_k}\nabla\cdot(\rho_k U_k v_k)dV = -\int_{V_k}\nabla\cdot\underline{q}_k dV - \int_{V_k}\left(P_k\underline{\underline{I}} - \underline{\underline{\tau}}_k\right):\nabla\underline{v}_k dV + \int_{V_k}Q_k dV \quad (15)$$

Applying the Leibnitz rule to the first term in equation (15), equation (16) is obtained.

$$\int_{V_k}\frac{\partial\rho_k U_k}{\partial t}dV = \frac{\partial}{\partial t}\int_{V_k}\rho_k U_k dV - \int_{A_s}\rho_k U_k\underline{v}_s\cdot\underline{n}\,dA \quad (16)$$

Using the Gauss theorem again to the spatial divergence term in equation (15),

$$\int_{V_k}\nabla\cdot\left(\rho_k U_k v_k + \underline{q}_k\right)dV = \nabla\cdot\int_{V_k}\left(\rho_k U_k\underline{v}_k + \underline{q}_k\right)dV$$
$$+\int_{A_s}\left(\rho_k U_k\underline{v}_k + \underline{q}_k\right)\cdot\underline{n}\,dA + \int_{A_w}\underline{q}_k\cdot\underline{n}\,dA \quad (17)$$

where $\underline{v}_k\cdot\underline{n}=0$ due to of the no-slip condition.

After rearranging equations (16) and (17), the following equation comes from equation (15):

$$\frac{\partial}{\partial t}\int_{V_k}\rho_k U_k dV - \int_{A_s}\rho_k U_k\underline{v}_s\cdot\underline{n}\,dA$$
$$+\nabla\cdot\int_{V_k}\left(\rho_k U_k\underline{v}_k + \underline{q}_k\right)dV + \int_{A_s}\left(\rho_k U_k\underline{v}_k + \underline{q}_k\right)\cdot\underline{n}\,dA + \int_{A_w}\underline{q}_k\cdot\underline{n}\,dA$$
$$= -\int_{V_k}\left(P_k\underline{\underline{I}} - \underline{\underline{\tau}}_k\right):\nabla\underline{v}_k dV + \int_{V_k}Q_k dV \quad (18)$$

When the volume and surface integral terms are rewritten using the Gauss and Green theorems as in the momentum equation, equation (19) can be obtained.

$$\frac{\partial}{\partial t}(\gamma_v\alpha_k\rho_k U_k)+\left(\frac{1}{V}\right)\nabla\cdot[V\gamma_v\alpha_k\rho_k U_k\underline{v}_k]$$
$$=-\left(\frac{1}{V}\right)\nabla\cdot\left[V\gamma_v\alpha_k\underline{q}_k\right]-\gamma_v\alpha_k P_k\nabla\cdot\underline{v}_k+\gamma_v\alpha_k\underline{\underline{\tau}}_k:\nabla\underline{v}_k+\gamma_v\alpha_k Q_k$$
$$+\gamma_v\left(\Gamma_k U_{sk}+\underline{q}_{sk}\cdot\underline{A}_s+\underline{q}_{wk}\cdot\underline{A}_w\right) \quad (19)$$

The pressure work term, $-\gamma_v\alpha_k P_k\nabla\cdot\underline{v}_k$, is expanded as follows [5]:

$$\gamma_v\alpha_k P_k\nabla\cdot\underline{v}_k=\left(\frac{1}{V}\right)P_k\nabla\cdot(V\gamma_v\alpha_k\underline{v}_k)+\left(\frac{1}{V}\right)P_k\int_{A_s}\underline{v}_k\cdot\underline{n}\,dA$$
$$=\frac{P_k}{V}\nabla\cdot(V\gamma_v\alpha_k\underline{v}_k)+\frac{P_k}{V}\int_{A_s}\frac{\rho_k(\underline{v}_k-\underline{v}_s)}{\rho_k}\cdot\underline{n}\,dA+\frac{P_k}{V}\int_{A_s}\underline{v}_s\cdot\underline{n}\,dA$$
$$=\frac{P_k}{V}\nabla\cdot(V\gamma_v\alpha_k\underline{v}_k)-P_k\gamma_v\frac{\Gamma_k}{\rho_k}+P_k\gamma_v\left(\frac{\partial\alpha_k}{\partial t}\right) \quad (20)$$

The energy convection term can be assumed as the sum of the mean convection and the product of the fluctuating velocity and energy. The product term of the fluctuating quantity is neglected as in equation (21),

$$\overline{U_k\underline{v}_k}=\underline{\underline{K}}_k^U\cdot U_k\underline{v}_k+U_k'\underline{v}_k'\approx\underline{\underline{K}}_k^U\cdot U_k\underline{v}_k=U_k\underline{v}_k \quad (21)$$

where $(\underline{\underline{K}}_k^U)$ is the unit covariance term of which the magnitude is one.

By including the pressure work term and convection term obtained via equations (20) and (21), equation (18) can be rewritten as follows using the divergence theorem:

$$\frac{\partial}{\partial t}(\alpha_k\rho_k U_k)+\frac{1}{\gamma_v}\nabla(\gamma_a\alpha_k\rho_k U_k\underline{v}_k)$$
$$=-P_k\left[\frac{\partial\alpha_k}{\partial t}+\frac{1}{\gamma_v}\nabla(\gamma_a\alpha_k\underline{v}_k)\right]+\Gamma_k(U_{sk}+P_k/\rho_k)-\frac{1}{\gamma_v}\nabla(\gamma_a\alpha_k\underline{q}_k')$$
$$+\underline{q}_{sk}\cdot\underline{A}_s+\underline{q}_{wk}\cdot\underline{A}_w+\alpha_k Q_k+\alpha_k\mu_k(\nabla\underline{v}_k:\nabla\underline{v}_k) \quad (22)$$

The q' term contains the conduction contribution when S_c is occupied by the phase. In addition, it represents the Reynolds heat flux (turbulent thermal mixing) and the heat addition by the walls if S_c is a solid boundary wall. The thermal diffusivity terms were added to the energy equation for thermal stratification or inter-cell mixing flows. This also applies for as well as the lateral convective energy transfer terms. The turbulent heat flux and internal phasic heat transfer terms are considered as follows,

$$\frac{1}{\gamma_v}\nabla\left(\gamma_a\alpha_k\underline{q}_k'\right)=\frac{1}{\gamma_v}\nabla\left[\gamma_a\alpha_k\left(\underline{q}_k+\underline{q}_k^T\right)\right]=-\frac{1}{\gamma_v}\nabla\left[\gamma_a\alpha_k\left(k_k+k_k^T\right)\nabla T_k\right] \quad (23)$$

where k_k is a thermal conductivity and k_k^T is a turbulent thermal conductivity for phase k. The multi-dimensional gas phase energy equation adopting these modifications is

$$\frac{\partial\alpha_g\rho_g U_g}{\partial t}+\frac{1}{\gamma_v}\left[\frac{\partial}{\partial x}\left(\gamma_a\alpha_g\rho_g U_g u_g\right)+\frac{\partial}{\partial y}\left(\gamma_a\alpha_g\rho_g U_g v_g\right)+\frac{\partial}{\partial z}\left(\gamma_a\alpha_g\rho_g U_g w_g\right)\right]$$
$$=-P\frac{\partial\alpha_g}{\partial t}-\frac{P}{\gamma_v}\left[\frac{\partial\gamma_a\alpha_g u_g}{\partial x}+\frac{\partial\gamma_a\alpha_g v_g}{\partial y}+\frac{\partial\gamma_a\alpha_g w_g}{\partial z}\right]$$
$$+\frac{1}{\gamma_v}\left[\frac{\partial}{\partial x}\left(\gamma_a\alpha_g(k_g+k_g^T)\frac{\partial T}{\partial x}\right)+\frac{\partial}{\partial y}\left(\gamma_a\alpha_g(k_g+k_g^T)\frac{\partial T}{\partial y}\right)+\frac{\partial}{\partial z}\left(\gamma_a\alpha_g(k_g+k_g^T)\frac{\partial T}{\partial z}\right)\right]$$
$$+Q_{wg}+Q_{ig}+\Gamma_{ig}h_g^*+\Gamma_w h_g'+Diss_g \quad (24)$$

where

$$h_g^*=\begin{cases}h_g^s,\Gamma_g\geq 0\\ h_g,\Gamma_g<0\end{cases},\ h_g'=\begin{cases}h_g^s,\Gamma_w\geq 0\\ h_g,\Gamma_w<0\end{cases},\ h_f^*=\begin{cases}h_f,\Gamma_g\geq 0\\ h_f^s,\Gamma_g<0\end{cases},\ \text{and}\ \ h_f'=\begin{cases}h_f,\Gamma_w\geq 0\\ h_f^s,\Gamma_w<0\end{cases} \quad (25)$$

For the MARS multi-dimensional component, the main interests is an explanation of the effects of the inter-cell shear for a coarse multi-dimensional flow field. In addition, a time-consuming calculation scheme is not a suitable choice because MARS is a nuclear power plant system analysis code. Implying a zero equation turbulence model is feasible due to these considerations.

The turbulent terms in the multi-dimensional component only represent the force acting on the cell surface between the control volumes, as the wall drag is accounted for in the MARS one-dimensional equation. In the zero equation turbulence models, Prandtl's mixing length model is adapted in the MARS multi-dimensional component [16,17]. The applied turbulent viscosity μ_T and turbulent conductivity k_T are expressed as

$$\mu_T=\rho l_m^2\sqrt{2\underline{\underline{D}}^*:\underline{\underline{D}}^*} \quad (26)$$

$$k_T=\rho C_P\varepsilon_T=\rho C_P l_h l_m\sqrt{2\underline{\underline{D}}^*:\underline{\underline{D}}^*} \quad (27)$$

where l_m and l_h are the momentum and energy mixing length as defined by a-user input, respectively. ε_T is the turbulent dissipation rate, and And $\underline{\underline{D}}^*$ is the deleted bulk deformation tensor [18]. It is rewritten as follows:

$$\underline{\underline{D}}^{*} = \frac{1}{2}\begin{pmatrix} 0 & \frac{\partial u}{\partial y}+\frac{\partial v}{\partial x} & \frac{\partial u}{\partial z}+\frac{\partial w}{\partial x} \\ \frac{\partial v}{\partial x}+\frac{\partial u}{\partial y} & 0 & \frac{\partial v}{\partial z}+\frac{\partial w}{\partial y} \\ \frac{\partial w}{\partial x}+\frac{\partial u}{\partial z} & \frac{\partial w}{\partial y}+\frac{\partial v}{\partial z} & 0 \end{pmatrix} \tag{28}$$

The directional velocity derivatives are formulated in the a finite difference form with a discrete grid and with velocity notations. Equations for the cylindrical coordinates are also implemented in the multi-dimensional component of MARS.

3. MULTI-DIMENSIONAL SOLUTION SCHEME

In the one-dimensional MARS code, the numerical solution scheme is based on a semi-implicit, finite-difference method using a staggered-grid mesh and a donor-cell scheme [16]. The same numerical solution scheme is used for the multi-dimensional equation.

Added terms can be implemented easily because explicit velocity gradients are used in the multi-dimensional semi-implicit scheme. Figure 2 shows a staggered-grid mesh in Cartesian coordinates for the x-y plane, in which the velocities are defined at the cell surface (or junctions, j, k, $j+1$, $k+1$, etc.) and where the other scalar variables are at the cell centers (K, L, M).

After finite difference discretization, the multi-dimensional convection term is obtained in the following form:

$$\frac{1}{\gamma_v}\left(\frac{\alpha_g\rho_g\gamma_{a,x}}{2}\frac{\partial u_g^{\,2}}{\partial x}+\alpha_g\rho_g\gamma_{a,y}v_g\frac{\partial u_g}{\partial y}+\alpha_g\rho_g\gamma_{a,z}w_g\frac{\partial u_g}{\partial z}\right)$$

$$=\left[\frac{\left(\alpha_g^{*}\rho_g^{*}\right)_j^n\left(\gamma_a\bar{u}_g u_g^{*}\right)_i^n-\left(\alpha_g^{*}\rho_g^{*}\right)_j^n\left(\gamma_a\bar{u}_g u_g^{*}\right)_K^n}{2\gamma_v\Delta x_{j,k,l}}\right]+\left[\frac{\left(\alpha_g^{*}\rho_g^{*}\right)_j^n\left(u_g^{*}\right)_j^n\bar{v}_{g,k+1}^{n}-\left(\alpha_g^{*}\rho_g^{*}\right)_j^n\left(u_g^{*}\right)_j^n\bar{v}_{g,k}^{n}}{\gamma_v\Delta y_{j,k,l}}\right]$$

$$+\left[\frac{\left(\alpha_g^{*}\rho_g^{*}\right)_j^n\left(u_g^{*}\right)_j^n\bar{w}_{g,l+1}^{n}-\left(\alpha_g^{*}\rho_g^{*}\right)_j^n\left(u_g^{*}\right)_j^n\bar{w}_{g,l}^{n}}{\gamma_v\Delta z_{j,k,l}}\right] \tag{29}$$

where the variables with asterisks indicate the donor quantities, and the bar indicates the average value of two adjacent junctions in that direction. Following these notations, the y-directional average velocities for junctions k and $k+1$ can be represented as follows:

$$\bar{v}_{g,k+1}^{n}=\frac{1}{2}\left(\gamma_a v_{g,j,k+1,l}^{n}+\gamma_a v_{g,j-1,k+1,l}^{n}\right)$$

$$\bar{v}_{g,k}^{n}=\frac{1}{2}\left(\gamma_a v_{g,j,k,l}^{n}+\gamma_a v_{g,j-1,k,l}^{n}\right) \tag{30}$$

In addition to the convection term, the diffusivity term is expanded in a finite difference form. The finite difference

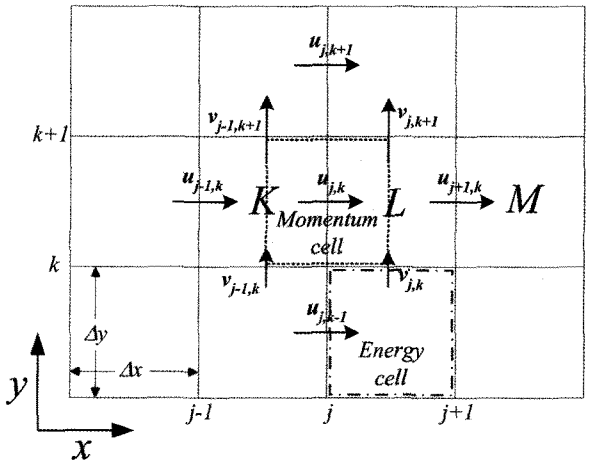

Fig. 2. The Multi-dimensional Staggered-grid Mesh at the$l$ Level

form of the momentum diffusion term in an x-directional flow is given by

$$\frac{(\mu_g+\mu_{g,T})}{\gamma_v}\left[\gamma_{a,y}\frac{\partial^2 u_g}{\partial y^2}+\gamma_{a,z}\frac{\partial^2 u_g}{\partial z^2}\right]$$

$$=\frac{\mu+\mu_T}{2\gamma_v\Delta y_{j,k,l}}\left[\left(\gamma_{a,y}^{k+}\frac{u_{j,k+1,l}-u_{j,k,l}}{\Delta y_{j,k+1,l}}+\gamma_{a,y}^{K+}\frac{u_{j,k+1,l}-u_{j,k,l}}{\Delta y_{j,k+1,l}}\right)-\left(\gamma_{a,y}^{k-}\frac{u_{j,k,l}-u_{j,k-1,l}}{\Delta y_{j,k,l}}+\gamma_{a,y}^{K-}\frac{u_{j,k,l}-u_{j,k-1,l}}{\Delta y_{j,k,l}}\right)\right]^n$$

$$+\frac{\mu+\mu_T}{2\gamma_v\Delta z_{j,k,l}}\left[\left(\gamma_{a,z}^{k+}\frac{u_{j,k,l+1}-u_{j,k,l}}{\Delta z_{j,k,l+1}}+\gamma_{a,z}^{K+}\frac{u_{j,k,l+1}-u_{j,k,l}}{\Delta z_{j,k,l+1}}\right)-\left(\gamma_{a,z}^{k-}\frac{u_{j,k,l}-u_{j,k,l-1}}{\Delta z_{j,k,l}}-\gamma_{a,z}^{K-}\frac{u_{j,k,l}-u_{j,k,l-1}}{\Delta z_{j,k,l}}\right)\right]^n \tag{31}$$

The thermal diffusion term in the multi-dimensional energy equation can also be extended easily to a finite difference form using a donor formulation; it is and approximated explicitly by a central difference scheme.

The MARS code has a modular data structure for its volume and junctions [5,11]. New member variables of four adjacent junction indices were added for the multi-dimensional junction variable groups. The multi-dimensional junction using these variables defines a three-dimensional array of volumes along with the internal flow path-way of these volumes. The MARS solver includes these additional junctions in the same manner used with the one-dimensional junctions treatment. After obtaining the solutions, the junctions are interpreted in terms of their directional information .

4. MODIFICATION FOR A STRATIFIED FLOW

Traditional vertical and/or horizontal flow regime maps are used for the one-dimensional component of MARS. For the multi-dimensional volume, the flow regimes are determined by the traditional criteria as well as by the elevation angle of the mass flux. In a one-dimensional component, the component angle input is directly compared to the gravitation and the elevation angle of the volume.

The elevation angle of the multi-dimensional component ϕ is defined as

$$\phi = \cos^{-1}\left(\frac{\vec{g}_x G_x + \vec{g}_y G_y + \vec{g}_z G_z}{G_m}\right) \quad (32)$$

where the mass flux G, gravitational force g and its directional vectors for the multi-dimensional volumes are defined as follows:

$$G_m = \sqrt{G_x^2 + G_y^2 + G_z^2} \quad (33)$$

$$g_T = \sqrt{g_x^2 + g_y^2 + g_z^2} \quad (34)$$

$$\vec{g}_x = g_x / g_T,\ \vec{g}_y = g_y / g_T, \text{ and } \vec{g}_z = g_z / g_T \quad (35)$$

The transition criteria for the multi-dimensional volumes use the same criteria used with the one-dimensional volumes. However, a direct application of the one-dimensional criterion to the horizontal stratifications may result in an unphysical flow field. For piled of volumes, horizontal stratification only occurs in the upper interface volumes. Thus the volume inside the bulk space of the multi-dimensional component ignores horizontal stratification even when the vapor volume fraction meets the stratification criterion.

Therefore, a new criterion for horizontal stratification is necessary in the multi-dimensional volumes. It is defined as follows:

- Horizontal stratification is only allowed if there is such a steep void profile in the vertical direction of the piled volumes that the void fraction in the lower cell is less than 0.1 and the void fraction in the upper cell is greater than 0.9 [4].

5. FUNDAMENTAL ASSESSMENT

For the first series of assessments, mass and energy conservations were tested and the basic symmetric flow problem was evaluated for all directional flows. In addition, several well-known conceptual problems which have an analytical solution were selected and analyzed. These assessments showed that the 3D terms were correctly implemented in the MARS code [15,19,20]. Table 2 shows the assessment matrix for the MARxS multi-dimensional component [15].

After these basic tests, separate effect tests were simulated and compared with the experimental data and other 3D code results. Among these items, two different separate effect tests are described below. The first assessment subject is the prediction capability of the multi-dimensional void distribution. The second assessment subject is the prediction capability of the multi-dimensional flow distribution as well as that for multi-dimensional flow splitting.

5.1 RPI Air-Water Experiment

Air-water two-phase experiments were performed with a two-dimensional test section in a low-pressure loop by RPI (the Rensselaer Polytechnic Institute) [21,22]. This test section simulates the core of a pressurized water reactor

Table 2. Assessment Matrix for the MARS Multi-dimensional Component

Test Problems	Test Objectives
1. Conceptual Problems	
The rigid body rotation problem	The azimuth momentum flux terms
The pure radial symmetric flow problem	The radial momentum flux terms
The gravity wave problem	Mass & momentum distribution in a 3D space
The tank drain problem	
The basic heat conduction problem	Heat conduction term in energy eqs.
2. Separate Effect Test or Comparison of the CFD code results	
2D Rectangular Plenum Mixing	Single-phase turbulent mixing
RPI Air-water Experiments	Two-phase multi-dimensional behavior
UPTF Test 7	ECC Bypass multi-dimensional behavior
KAERI MIDAS ECC Bypass Test	
3. Plant Application (to be done)	
APR1400	Full-3D Plant Application

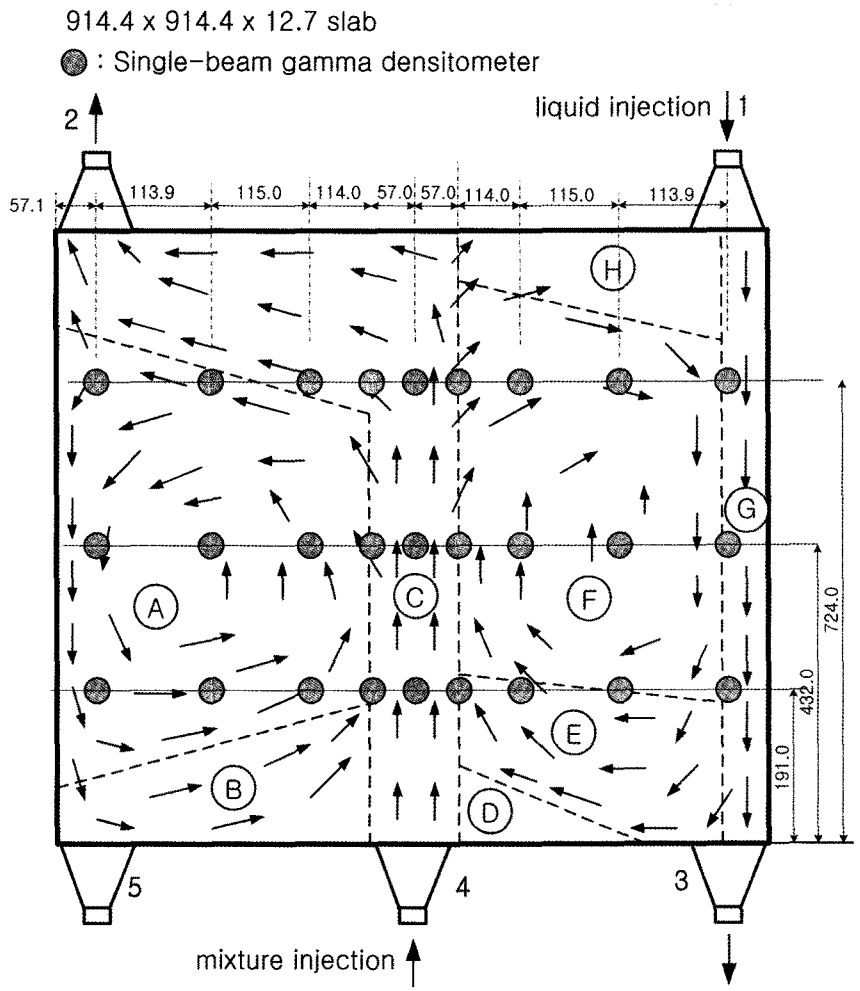

Fig. 3. RPI Test Section and Qualitative Flow Patterns [14]
[(A)Bubbly/Slug, (B),(D)Single-phase, (C)Slug, (E)Bubbly, (F)Bubbly/Slug, (G)Pure Liquid, (H)Air-pocket]

through a vertical two-dimensional slice channel. Originally, there were 36 different test cases according to the injection conditions and the presence of internal obstacle rods in the test section. A rectangular slab 36 inches by 36 inches square with a depth of 0.5 inches was used. The void fractions were measured with a traversing single-beam gamma densitometer. Twenty-seven measurement positions were determined located toformulate the void fraction distribution of the test section. Figure 3 shows the test section geometry and the qualitative flow patterns. The locations of the measurements are illustrated. The measurement locations are grouped into three sets with respect to the height from the bottom inside of the test section.

Only the '2AN4' case was selected from among the tests because there were no significant differences between the measured void fractions that MARS could resolve. The 2AN4 test case has two inlet ports and two outlet ports. A single-phase liquid was supplied from Port 1 in the upper right corner. A two-phase mixture was supplied to Port 4 at the bottom center of the test section. Ports 2 and 3 are outlets for the two-phase mixtures from the upper left and lower right corners. There is no flow at Port 5. The total liquid flow rate is 1.18 kg/s, the flow split fraction of Ports 1 and 4 is 0.5, and the air flow rate is 0.00547 kg/s for Port 4. The system pressure was maintained at 31.6 kPa.

The test procedure involved filling the test section with liquid. supplying a liquid flow to Ports 1 and 4, and establishing an air flow to Port 4. The flow rates were adjusted with flow control valves.

Figure 4 shows that the MARS modeling consists of a 17×17 rectangular multi-dimensional slab connected by four time-dependent boundary volumes. The internal volumes use no wall friction terms. Instead, a viscosity term which calculated by Prandtl's mixing length model is applied.

The results are shown in Figures 5 and 6. The calculated void fractions are compared with the measured void

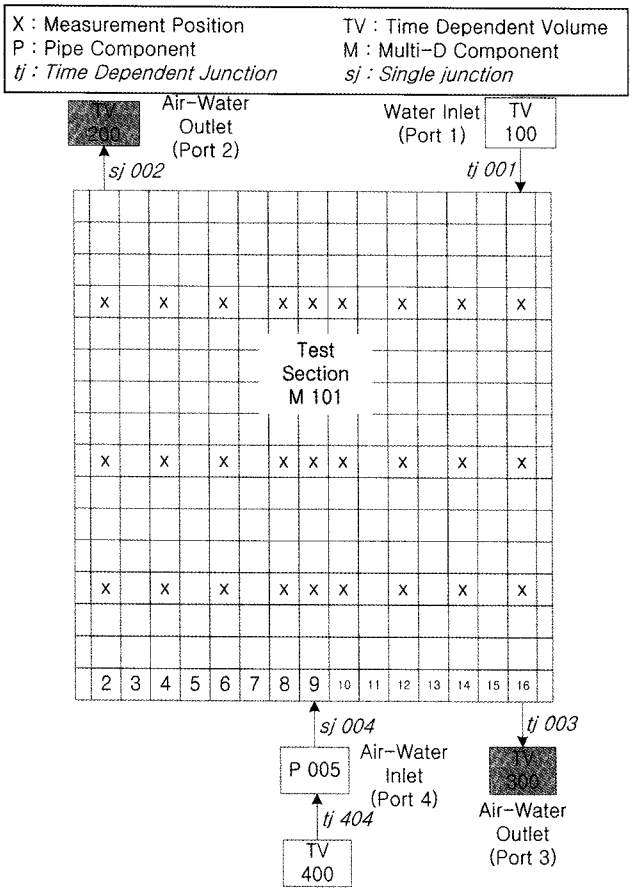

Fig. 4. Nodalization for the RPI Air-water Test: "X" Represents a Void fraction Measurement Positions

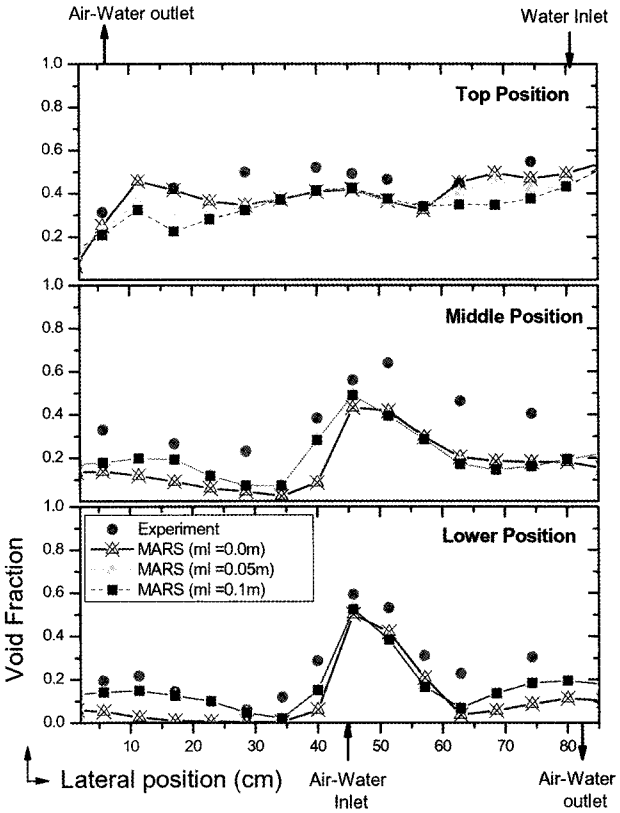

Fig. 5. Comparison of the MARS Results with the Measured Void Fractions

fraction in Figure 5. It was found that the predicted two-phase flow patterns and the void fraction profiles are in good agreement with the measured data. However, less prediction capability was observed in the distant region of the fluid injection or outlet ports. In the middle right region and the top center region, relatively large differences between the MARS calculation and measurements are observed.

The effect of the mixing length input is not significant. With a zero mixing length, the turbulent viscosity term is neglected in the momentum equation. When the mixing lengths vary between 0.05 and 0.1, negligible differences are observed in the predicted void fractions.

5.2 UPTF Test 7 ECC Bypass Test

The Upper Plenum Test Facility (UPTF) was designed and constructed for simulations of the 1300 MWe four-loop PWR of Siemens-KWU [23,24]. The objective of the UPTF program was a full-scale investigation of the 3D single and two-phase flow behaviors in the primary system of a PWR during the end-of-blowdown, refill, and reflood phases of a LOCA. Among the UPTF tests,

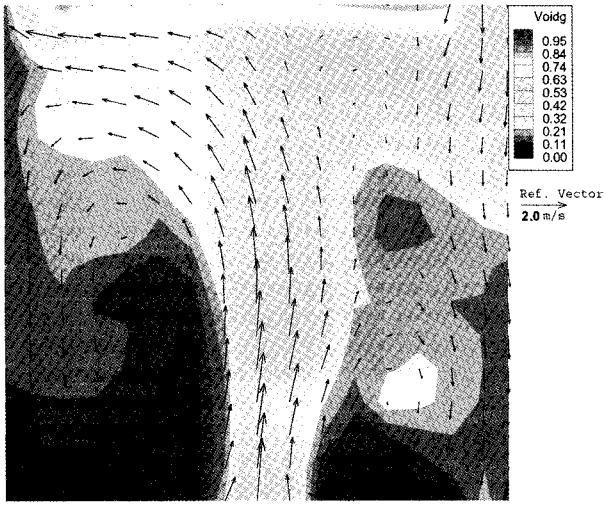

Fig. 6. MARS Result of the Void Fraction Profile and Flow Pattern

downcomer Test 7 was selected for the assessment for the MARS multi-dimensional component. As this test was carried out under nearly saturated conditions, the flow behaviors in the downcomer were mainly governed

Table 3. Experimental Conditions of the UPTF Test 7

Test /Phase	Steam injection (kg/s)	Steam temp. (K)	ECC flow in cold legs			ECC subcooling (K)	ECC delivery (kg/s)	Pressure in D/C (kPa)
			1 (kg/s)	2 (kg/s)	3 (kg/s)			
201/III	102	455.2	493	487	489	12	942	414
203/IV	51	461.2	493	485	487	2	1031	337
200/I	104	471.2	494	0	0	20	5	451
201/I	102	468.2	0	487	490	10	861	330
202/II	128	463.2	0	486	491	11	714	416
200/III	102	467.2	735	0	0	22	6	498
203/III	71	464.2	737	0	733	9	823	398
203/I	69	471.2	735	0	0	13	95	401
200/II	54	469.2	736	30	0	7	351	330
203/II	30	468.2	737	0	0	0	519	286

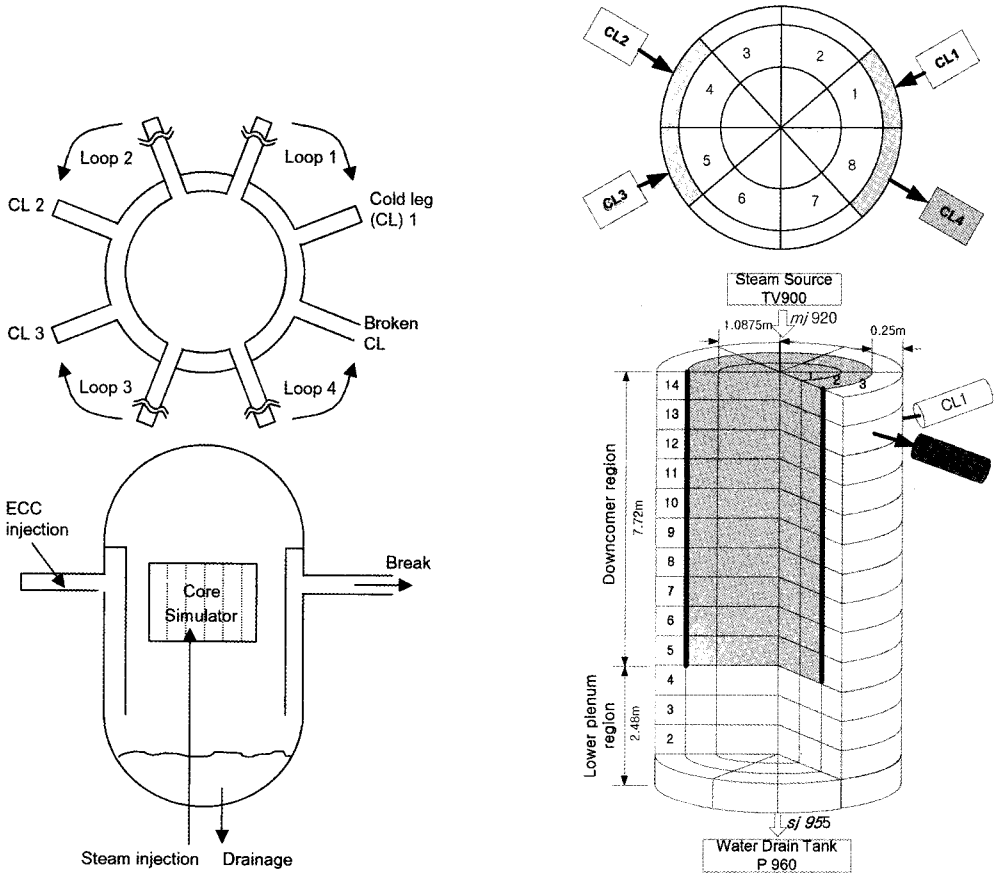

Fig. 7. Schematic of the UPTF Test 7 Experimental Facility and the MARS Input Model

by the mechanical interactions between the steam and water. The effect of condensation was not great in Test 7.

The UPTF Test 7 is a quasi-steady-state experiment that is performed to obtain full-scale data on the downcomer and lower plenum refill behavior of low steam flows. In the tests, steam and nearly saturated ECC water were injected from the core simulator and the cold legs at controlled rates, respectively, to determine the penetration

of ECC water into the downcomer and lower plenum as a function of the upward steam flow in the downcomer. To analyze the effects of the cold-leg arrangement on the ECC bypass phenomena, the ECC was injected into the cold legs with various combinations. The test consisted of four runs, numbered from 200 through 203, and each run had several phases distinguished by different steam and ECC flows, as listed in Table 3. The UPTF system configuration for Test 7 is given in Figure 7. The water level was maintained below the critical level via drainage at the bottom of the lower plenum. The critical water level depended on the upward steam flow rate.

The boundary and initial conditions of Test 7 were as follows:

- Hot-leg break valve: Closed
- Cold-leg break valve: Fully open
- All pump simulators: Closed
- Secondary side: Isolated
- Steam flow to the core simulator: Regulated as a function of time

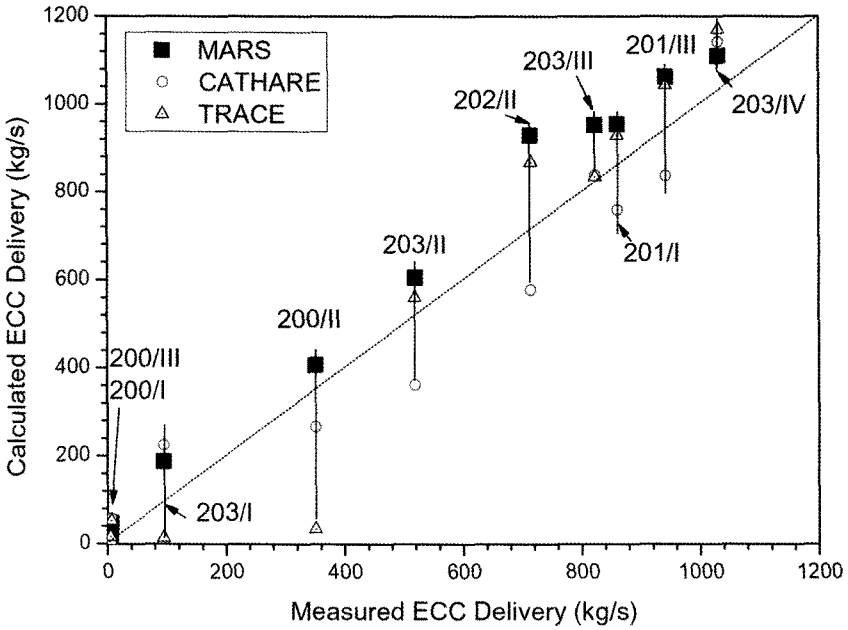

Fig. 8. Calculation Results for the ECC Delivery Flow of the UPTF Test 7

Table 4. The UPTF Test 7 ECC Delivery Simulation and Measurement Results

Test/Phase	ECC delivery (kg/s)			
	Experiment	MARS	CATHARE	TRACE
201/III	942	1062.75 (12.8)	837 (-11.1)	1044 (10.8)
203/IV	1031	1110.41 (7.7)	1142 (10.7)	1170 (13.5)
200/I	5	11.62 (132.4)	0 (-)	16.23 (225)
201/I	861	955.13 (10.9)	759 (-11.8)	928.74 (7.9)
202/II	714	929.67 (30.2)	578 (-19.0)	868 (21.6)
200/III	6	48.02 (700)	58 (867)	52.46 (774)
203/III	823	952.72 (15.8)	839 (1.9)	835 (1.5)
203/I	95	187.22 (97.1)	226 (138)	14.06 (-85.2)
200/II	351	407.87 (16.2)	267 (-23.9)	34.9 (-90.1)
203/II	519	605.98 (16.8)	362 (-30.3)	560.2 (7.9)

( ): percentage difference from the experimental results

- ECC flows: Regulated as a function of time
- Drainage from the lower plenum: Regulated to maintain the water level below a certain limit
- Initial system pressure: 2.5 bar
- Break pressure: Kept constant at 2.5 bar

The UPTF reactor vessel simulator was modeled using a multi-dimensional component, as shown in Figure 7. Cylindrical coordinates of the multi-dimensional component were used. The downcomer region was modeled using eight sectors with ten vertical nodes. The lower plenum possesses four vertical nodes. At the bottom of the lower plenum, a one-dimensional pipe was connected. In addition, a time-dependent junction was connected to the end of the pipe. This time-dependent junction was used to keep the lower plenum water level below a critical value by regulating the drainage flow. The reactor vessel wall was not modeled, as its thermal effects are not important in the downcomer Test 7. The turbulent mixing length input was 0.0; hence, the simulation was performed without the effect of viscosity. No modification of the wall or interfacial friction model was assigned. Table 4 summarizes the test and calculation results of the multi-dimensional system analysis codes TRACE [25] and CATHARE [26] as well as those of MARS [24]. Figures 8 shows the ECC water delivery data compared to the measured data as well as the results of other system codes that have a multi-dimensional capability. CATHARE regularly underestimated the UPTF Test 7 results, except for Run 203/I and 203/IV. TRACE showed prediction results similar to those of MARS in high-ECC delivery cases. However, in the low-ECC delivery cases, the delivery amounts predicted by TRACE were very low. The cases of Run 203/I, 203/II and 200/II were predicted to have less differences by the MARS code. In these cases, most of the ECC water was injected into cold leg 1, that is, close to the broken cold leg. However, in the Run 201/I and Run 202/II cases, the ECC was injected into legs 2 and 3, which were both far from the broken cold leg. MARS overestimates the ECC delivery by 10 % ~ 30 %. This indicates that the prediction of the ECC delivery strongly depends on the ECC injection location.

6. CONCLUSION

A multi-dimensional component was developed for MARS to predict multi-dimensional flow behaviors. The governing equations for the multi-dimensional component were extended from a one-dimensional module. Lateral convection and diffusion terms were implemented into the momentum and energy equations, respectively. Multi-dimensional components can be applied with Cartesian and cylindrical coordinates. This allows for more flexible capabilities of multi-dimensional flow analysis as a best-estimate system analysis code.

After the validation of the implemented multi-dimensional terms, separate effect tests were simulated to verify the multi-dimensional component. The calculated results of the RPI air-water experiment demonstrated good prediction capability for the void fraction of a multi-dimensional mixture flow. The simulation results of UPTF Test 7 were also compared with those of other multi-dimensional system codes with respect to the mass distribution and splitting. MARS overestimated the ECC delivery by 10 % ~ 30 %. CATHARE generally underestimated the UPTF Test 7 results, apart from Run 203/I and 203/IV. TRACE showed prediction results that were similar to those of MARS in high-ECC delivery cases. However, in the low-ECC delivery cases, the delivery amounts predicted by TRACE were very low.

Even when ignoring the non-drag interfacial forces, resolution of the multi-dimensional mass void distribution is sufficient for the length scale of a nuclear system safety analysis. Further assessments are required regarding the definitive use of the multi-dimensional capability of the MARS code. Additional experimental validation processes and the establishment of a handling method for the multi-dimensional flow regime should follow. Through these efforts, the use of the multi-dimensional capability of MARS would be enhanced and would lead to a better understanding of the multi-dimensional thermal-hydraulic phenomena in nuclear power plants.

ACKNOWLEDGEMENTS

This work was supported by the Nuclear Research & Development Program under a KOSEF (Korea Science and Engineering Foundation) grant funded by MEST (The Ministry of Education, Science and Technology) of the Korean government (Grant Code: M20706060002-08M0606-00210).

NOMENCLATURE

A	cross-sectional area (m^2)
B	body force (m/s^2)
C	virtual mass coefficient
C_p	specific heat capacity (J/kg/K)
$\underline{\underline{D}}^*$	deleted bulk deformation tensor (s^{-1})
$DISS$	energy dissipation function (W/m^3)
FWG	wall drag coefficients for vapor phase (s^{-1})
FIG	interface drag coefficients for vapor phase (s^{-1})
$\underline{g}$	body force vector (m/s^2)
h	enthalpy (J/kg)
$\underline{J}$	flux quantity of equation
$\underline{\underline{k}}$	thermal conductivity (W/m·K)
l	turbulent mixing length (m)
$\dot{m}$	mass flux (kg/m^2s)
n	normal vector
P	pressure (Pa)
Q	volumetric heat flux (W/m^3)
r	radius of cylinder (m)
U	internal energy (J/kg)
V	cell volume (m^3)
u,v,w	directional velocity (x,y,z or r,θ,z) (m/s)

Greek Symbols

α	fraction of each phase (f or g)
Γ	mass generation term (kg/s/m^3)
$\gamma_{a,k}$	surface fraction of k-direction face (A_k /A)
γ_v	volume fraction of a fluid, (V_f +V_g)/V
μ	viscosity (kg/m/s)
ρ	density (kg/m^3)
$\underline{\underline{\tau}}$	shear stress (N)
Δ	time average quantity, mesh interval

Subscripts

i	interface
j,k,l	cell edge of x-, y- and z-direction, respectively
f	liquid phase
g	vapor phase
k	any phase
m	mixture
tot	total
T	turbulence term
w	wall
s	boundary of meshes, solid wall

Superscripts

T	tubulent
*	bulk/saturation property
'	near wall property, fluctuation
-	averaged value

REFERENCES

[1] P. S. Damerell, *et. al.*, "Reactor Safety Issues Resolved by the 2D/3D Program," NUREG/IA-0127, USNRC report (1993).

[2] OECD Nuclear Agency, "Nuclear safety research in OECD countries, Summary Report on Capabilities and Facilities (SESAR/CAF)," OECD, Paris (1997).

[3] R. G. Steinke, V. Martinez, N. M. Schnurr, J. W. Spore, and J. V. Valdez, "TRAC-M/FORTRAN90 (Version3.0) User's Manual," LA-UR-00-834, Los Alamos National Laboratory (2000).

[4] J. M. Kelly, "TRAC-M Code Consolidation and Development," *Fall 2002 CAMP Meeting Sponsored by USNRC*, Alexandria, Virginia USA, Oct. 31, 2002.

[5] RELAP5-3D Development Team, "RELAP5-3D Code Manuals, Volumes I, II, IV, and V," INEEL-EXT-98-00834, Revision 1.1b, Idaho National Engineering and Environmental Laboratory (1999).

[6] F. Barre, I. Dor, and C. Sun, "The multi-dimensional module of CATHARE2. Description and application," *Proc. of the 7th International Topical Meeting on Nuclear Reactor Thermal-Hydraulics (NURETH-7)*, Saratoga Springs, USA, 1995.

[7] K.Takeuchi, M.E. Nissley, J.S. Spaargaren, and S.I. Dederer, "Scaling effects predicted by WCOBRA/TRAC for UPI plant best estimate LOCA," *Nuclear Engineering and Design*, **186**, pp.257-278 (1998).

[8] H.K. Cho, B.J. Yun, C.-H. Song, and G.C. Park, "Experimental validation of the modified linear scaling methodology for scaling ECC bypass phenomena in DVI downcomer," *Nuclear Engineering and Design*, **235**, pp.2310-2322 (2005).

[9] B.J. Yun, D.J. Euh, and C.-H. Song, "Downcomer boiling phenomena during the reflood phase of a large-break LOCA for the APR1400," *Nuclear Engineering and Design*, **238**, pp. 2064-2074 (2008).

[10] Seok Cho, Chul-Hwa Song, Choon-Kyong Park, Hwan-Yeol Kim, and Won-Pil Baek, "Air clearing pressure oscillation produced in a quenching tank by a prototype unit cell sparger of the APR1400," *Nuclear Engineering and Design*, **238**, pp.1525-1534 (2008).

[11] J.-J. Jeong, K. S. Ha, B. D. Chung, and W.J. Lee, "A Multi-Dimensional Thermal-Hydraulic System Analysis Code, MARS 1.3.1," *Journal of the Korean Nuclear Society*, **31**, pp.344-363 (1999).

[12] W. J. Lee, B. D. Chung, J.-J. Jeong, and K. S. Ha, "Development of a Multi-dimensional Realistic Thermal-Hydraulic System Analysis Code, MARS 1.3 and Its Verification," *Proc. NTHAS98: First Korea-Japan Symposium on Nuclear Thermal Hydraulics and Safety*, Busan, Korea, Oct. 21-24, 1998.

[13] J.-J. Jeong, K.S. Ha, B.D. Chung, W.J. Lee, "Development of a multi-dimensional thermal-hydraulic system code, MARS 1.3.1," *Annals of Nuclear Energy*, **26**, pp.1611-1642 (1999).

[14] J.J. Jeong, H.Y. Yoon, I.K. Park, H.K. Cho, J. Kim, "A semi-implicit numerical scheme for transient two-phase flows on unstructured grids," *Nuclear Engineering and Design*, **238**, pp.3403-3412 (2008).

[15] B. D. Chung, S. W. Bae, J.-J. Jeong, and S. M. Lee, "Development and assessment of the multi-dimensional flow models in the thermal-hydraulic system analysis code MARS," KAERI/TR-3011/2005, Korea Atomic Research Institute (2005).

[16] V. H. Ransom, "Course A–Numerical Modeling of Two-Phase Flows for Presentation at Ecoled'Ete d'Analyse Numerique," EGG-EAST-8546, Idaho National Engineering Laboratory (1989).

[17] M. J. Thurgood, J. M. Kelly, T. E. Guidotti, R. J. Kohrt, and K. R. Crowell, "COBRA/TRAC–A Thermal Hydraulics Code for Transient Analysis of Nuclear Reactor Vessels and Primary Coolant Systems," NUREG/CR- 3046, USNRC report (1983).

[18] M. Ishii and T. Hibiki, *Thermo-Fluid Dynamics of Two-Phase Flow*, pp. 169-186, Springer, (2006).

[19] K. E. Carlson, *et. al.*, "Developmental Assessment of the MultiDimensional Component in RELAP5 for Savannah River Site Thermal Hydraulic Analysis," EGG-EAST-9803 Rev. 0.0, Idaho National Engineering Laboratory (1992).

[20] B. D. Chung, *et. al.*, "Development and Assessment of Best Estimate Integrated Safety Analysis Code," KAERI/RR-2520/2004, Korea Atomic Energy Research Institute (2004).

[21] K. M. Bukhari and R. T. Jr. Lahey, "The Measurement of Countercurrent Phase Separation and Distribution in a Two-Dimensional Test Section," NUREG/CR-3577, Rensselaer Polytechnic Institute (1984).

[22] K.M. Bukhari and R.T. Lahey Jr., "An Experimental Study of 2-D Phase Separation Phenomena," *Int. J. Multiphase Flow*, **13**, No. 3, pp.387-402 (1987).

[23] H. Glaeser and H. Karwat, "The contribution of UPTF Experiments to Resolve Some Scale-Up Uncertainties in Countercurrent Two-Phase Flow," *Nucl. Eng. Design*, **145**,

63 (1993).
[24] K. Riedle, *et. al.*, "UPTF Test No. 7 Downcomer Countercurrent Flow Test," E314/90/003, Siemens KWU (1990).
[25] A. D. Shin, *et. al.*, "TRACE Code Assessment for Thermal Hydraulic Analysis in Direct Vessel Injection," KINS/RR-281, Korea Institute of Nuclear Safety (2004).
[26] J.-J., Jeong, I. Dor, and D. Bestion, "Improvement and assessment of CATHARE2 Three-dimensional module compared with the UPTF Downcomer test 7," *Nuclear Technology*, **117** (1997).